stle
LAS VEGAS
May 15-19, 2016

ELASTOGASDYNAMIC MODEL FOR AIR FOIL JOURNAL BEARINGS: HYSTERESIS PREDICTION INCLUDING PRELOADING EFFECTS

FLUID FILM BEARING VI – SESSION 6H

Marcel Mahner[a], Pu Li[a], Andreas Lehn[a], Bernhard Schweizer[a]
[a]Technical University Darmstadt, Department of Mechanical Engineering, Institute of Applied Dynamics

INTRODUCTION

Air foil journal bearings (AFJB) are frequently used to support shafts in rotating devices, for instance in micro gas turbines or in rotor systems for fuel cell applications, where oil-free bearings are mandatory. Air bearings have different advantages compared to oil journal bearings. They are simple and inexpensive to produce and they provide a minor maintenance effort. Due to the elastic foil structure, air foil journal bearings have the ability to accomodate journal misalignment and thermal growth.

In order to increase the stability of rotors supported by air foil journal bearings, three-pad configurations are often used instead of one-pad designs, see [1]. Three-pad air foil journal bearings consist of a rigid bearing sleeve and three pairs of bump and top foil, see Figure 1. The bump foil is a corrugated foil, which induces compliance and damping to the bearing. The top foil provides a smooth surface for the gasdynamic pressure generation.

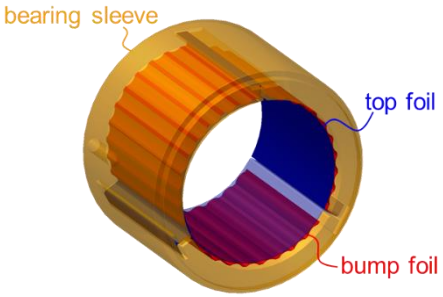

Fig. 1 Three-pad air foil journal bearing

For different reasons, an assembly preload of top and bump foil is introduced in air foil journal bearings which leads to a contact of top foil and rotor in case of a non-rotating, perfectly aligned rotor. In consequence of the assembly preload, the stiffness of the bearing for small rotor eccentricities as well as the overall bearing structural damping is increased. In order to predict the influence of the assembly preload on the gasdynamic pressure generation as well as on the bearing hysteresis, a detailed elastogasdynamic bearing model is mandatory.

In previous works, the deflections of bump and top foil were calculated using straightforward elastic foundation models [2, 3] or more detailed structural models [4-7]. In these works, preloading effects have not been taken into account.

In this paper, a detailed model of a preloaded three-pad air foil journal bearing is presented. With this model, the influence of the assembly preload on the gasdynamic pressure generation as well as on the bearing hysteresis is discussed in detail. For the purpose of model validation, a hysteresis measurement is carried out; the measured and the calculated hysteresis curves are compared.

ELASTOGASDYNAMIC MODEL

The elastogasdynamic model incorporates the description of the gasdynamic pressure generation in the convergent gap between top foil and rotor as well as the description of the elastic deformation of bump and top foil.

Assuming iso-thermal conditions and an ideal gas behavior, the pressure distribution in the gas film in each bearing pad (length L_t, width b_t) is described by the compressible Reynolds equation

$$\frac{1}{1+\varepsilon_{t_i}}\frac{\partial}{\partial s_t}\left(\frac{1}{1+\varepsilon_{t_i}}\frac{p_i h_i^3}{\eta}\frac{\partial p_i}{\partial s_t}\right)+\frac{\partial}{\partial z}\left(\frac{p_i h_i^3}{\eta}\frac{\partial p_i}{\partial z}\right)=-\frac{6\, r_R \Omega}{1+\varepsilon_{t_i}}\frac{\partial (p_i h_i)}{\partial s_t} \qquad \forall\, i=1,2,3 \tag{1}$$

assuming the boundary conditions

$$p_i(s_t=0,z)=p_i(s_t=L_t,z)=p_i(s_t,z=0)=p_i(s_t,z=b_t)=p_a \qquad \forall\, i=1,2,3. \tag{2}$$

Herein, p_i denotes the pressure in the i-th bearing pad. η terms the dynamic viscosity of air at a constant temperature. h_i is the gap function. r_R and Ω denote the radius and the rotational speed of the rotor. Furthermore, p_a terms the ambient pressure. Since the Reynolds equation is projected onto the deformed top foil surface, the elongation of the top foil in normal direction is accounted for by the factor $1/(1+\varepsilon_{t_i})$ in the Reynolds equation (1), where ε_{t_i} denotes the normal strain of each top foil. s_t and z are the tangential and axial coordinates of the top foil.

Assuming a constant foil thickness, Reissner-Mindlin kinematics and the plane strain assumption in axial bearing direction, the deformation of bump and top foil is described by the nonlinear 1D *Beamshell* theory according to Reissner [8, 9]. Since this theory is only one-dimensional, the 2D pressure distribution obtained from the Reynolds equation (1) is averaged in axial bearing direction. This yields a 1D pressure distribution $\bar{p}$. A geometrically

nonlinear theory is mandatory, since large deformations occur due to the assembly preload. While the deformations are large, it is assumed that the normal, shear and bending strains remain small. Figure 2 depicts the boundary conditions of top and bump foil at the leading and trailing edges.

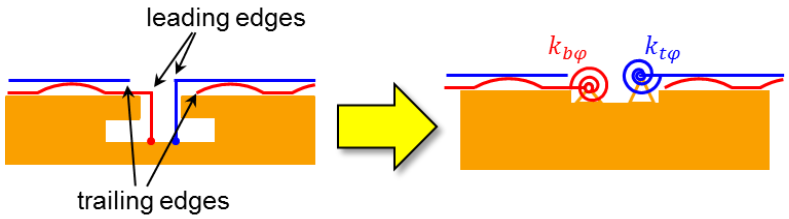

Fig. 2 Bump and top foil boundary conditions

The contact between bump and top foil as well as the contact between bump foil and bearing sleeve are modelled by a node-to-surface approach. The slave nodes for the contact between bump foil and bearing sleeve are the end points of each bump. For the contact between bump foil and top foil, the center points of each bump are used as slave nodes, see Figure 3a) and 3b). The no-penetration condition in normal direction is enforced using an augmented Lagrange approach [10, 11] which allows for the separation of bump and top foil. In tangential direction, the friction force is calculated using Coulomb's law of friction. The signum function in the friction law is regularized using an elastic slip approach, see Wriggers [11].

For the prediction of static hysteresis of foil air bearings, the rotational speed of the rotor is set to zero ($\Omega = 0$). Therefore, the rotor contacts the top foil surface. The contact between rotor and top foil is assumed to be frictionless due to the friction reduction coatings of top foil and rotor.

The governing set of differential and algebraic equations is solved using a finite element approach.

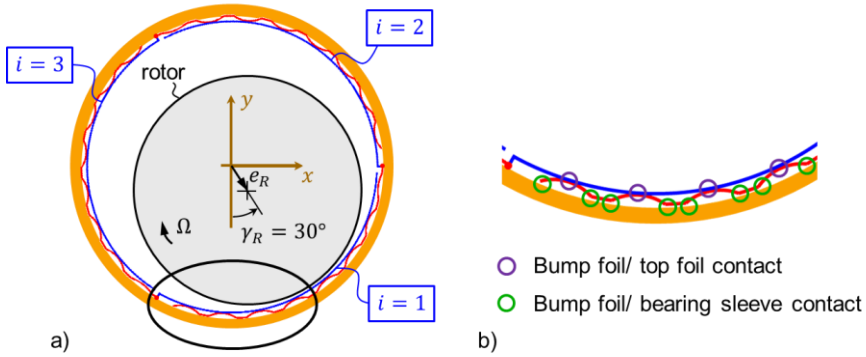

Fig. 3 Three-pad air foil journal bearing with rotor (a) and contact slave nodes on bump foil (b)

SIMULATION RESULTS

The effect of assembly preload on the gasdynamic pressure generation in a three-pad air foil journal bearing is discussed on basis of simulation results obtained with the above described model. In the simulation, the rotor spins at a constant rotational speed of $n = 60{,}000\,\mathrm{rpm}$. The rotor is quasi-statically moved with the harmonic function $e_R = \hat{e}_R/2\,[1 - \cos(2\pi t)]$ over two periods in the direction of the top foil center of the first air foil bearing pad (rotor angle $\gamma_R = 30°$), see Figure 3a). Herein, $\hat{e}_R$ terms the amplitude of the harmonic rotor displacement. Since inertia effects are neglected, t can be regarded as non-dimensional parameter. The calculation has been accomplished with $p_a = 1\,\mathrm{bar}$, $\eta = 19.25 \cdot 10^{-6}\,\mathrm{Pa\,s}$ (at $T_a = 311.11\,\mathrm{K}$) and $\hat{e}_R = 52\,\mu\mathrm{m}$.

Figure 4 shows the average pressure $\bar{p}_1$ (Figure 4a) and 4c)) as well as the shear force Q_{t_1} and the gap function h_1 (Figure 4b) and 4d)) over the non-dimensional top foil coordinate $\bar{s}_{t1} = s_{t_1}/L_t$ at $t_1 = 1$ and $t_2 = 1.5$ for the first air foil bearing pad. As can be seen from Figure 4a) and 4c), the pressure p_1 increases significantly while the rotor is displaced from $e_R(t_1) = 0\,\mu\mathrm{m}$ to $e_R(t_2) = \hat{e}_R = 52\,\mu\mathrm{m}$ due to the decreasing fluid film height, see Figure 4b) and 4d). At the maximum rotor displacement $e_R(t_2) = \hat{e}_R = 52\,\mu\mathrm{m}$, the pressure distribution $\bar{p}_1$ as well as the gap function h_1 show significant ripples, see Figure 4c) and 4d). These ripples are caused by the sagging of the top foil between neighboring bumps. Since the pressure is small for $e_R(t_1) = 0\,\mu\mathrm{m}$ and not all bumps are in contact either with the top foil or with the bearing sleeve, there is no visible sagging effect, see Figure 4b).

Figure 4b) and 4d) show the distribution of the top foil shear force Q_{t_1} over the non-dimensional top foil coordinate $\bar{s}_{t_1}$. The discontinuities are caused by the contact between bump and top foil. As can be seen from Figure 4b) and 4d), the

number of contact points between bump and top foil as well as the contact normal forces increase while the rotor is displaced. At $t_1 = 1$, the top foil contacts four bumps while at $t_2 = 1.5$ all bumps - except the bump near the top foil trailing edge - are in contact with the top foil.

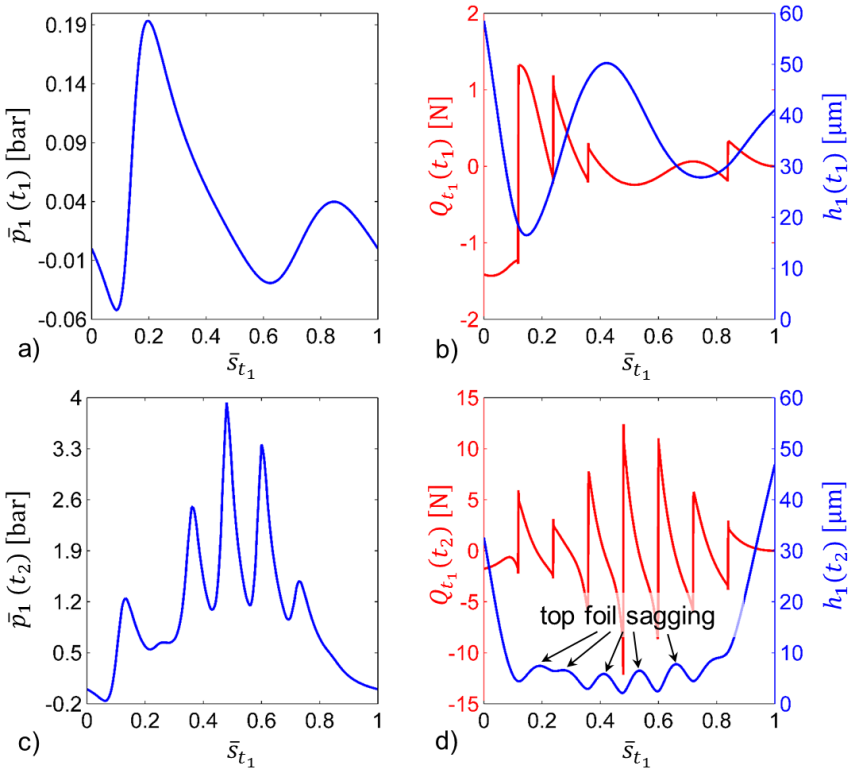

Fig. 4 Average Pressure (a, c) as well as top foil shear force and gap function (b, d) over the top foil non-dimensional coordinate for $e_R(t_1 = 1) = 0\ \mu m$ (a, b) and $e_R(t_2 = 1.5) = 52\ \mu m$ (c, d)

Summarizing, the pressure distribution for the two different rotor displacements shows a totally different shape due to the assembly preload: For low rotor eccentricities not all bumps are in contact with either the top foil or the bearing sleeve. Therefore the stiffness of the elastic foil structure is relatively small. For this case, bump and top foil deform due to the gasdynamic pressure without visible sagging effects. For large rotor displacements, more bumps come into contact with the bearing sleeve. This leads to an increase of the stiffness of the elastic foil structure. Due to the higher pressure and the high stiffness of the bump foil for this case, the top foil sags between neighboring bumps.

MEASUREMENT AND PREDICTION OF STATIC HYSTERESIS

To validate the mathematical model of the elastic foil structure, a static hysteresis measurement of a preloaded three-pad air foil journal bearing is performed and the result is compared to a hysteresis prediction obtained with the presented numerical bearing model.

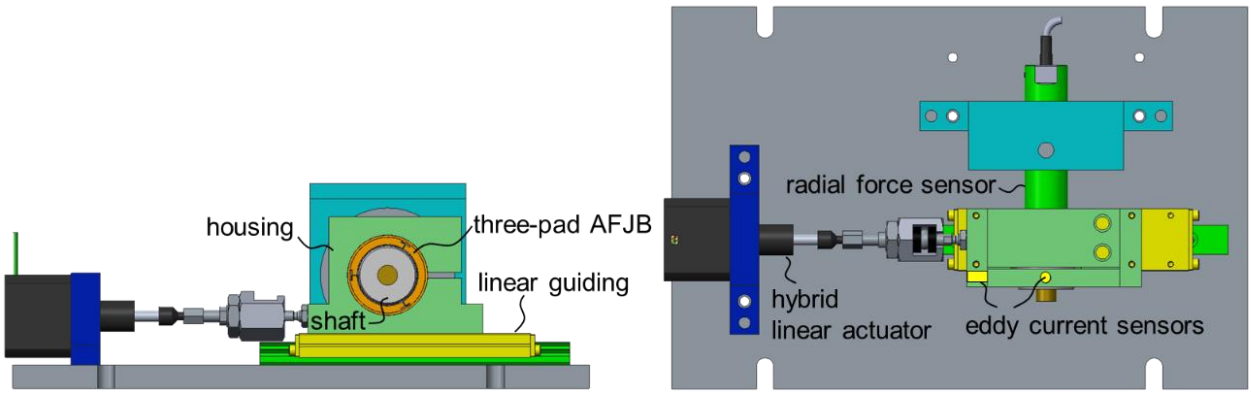

Fig. 5 Hysteresis device for the measurement of static hysteresis of air foil journal bearings

The measurement is accomplished with the hysteresis device shown in Figure 5. This device consists of a three-pad air foil journal bearing which is rigidly clamped in a housing. The housing is mounted on a linear guiding which can move in horizontal direction. The quasi-static displacement of the bearing relatively to the non-rotating shaft is induced by a hybrid linear actuator. The force on the shaft is measured with a radial force sensor that contains resistance strain gauges. The relative displacement of the bearing and the shaft is measured by two orthogonal eddy current sensors.

The prediction of the static hysteresis is achieved with the described bearing model by quasi-statically moving the non-rotating rotor with the harmonic function $e_R = \hat{e}_R \sin(2\pi t)$ over two periods in the direction of the top foil center of the first bearing pad (in y_1-direction, rotor angle $\gamma_R = 30°$), see Figure 6a).

Figure 6b) depicts the measured and the calculated static hysteresis curves for the described assembly orientation of the bearing. Herein, F_{y_1} denotes the force on the shaft in direction of the relative displacement. The hysteresis curves show a nearly constant stiffness for a wide range of the rotor displacement. This is caused by the assembly preload. As the rotor displacement increases, more bumps contact the bearing sleeve which leads to an increase in the stiffness of the elastic foil structure. Measurement and prediction agree well. Nevertheless, the transition from the area of small stiffness to the area of high stiffness is smoother in the measured hysteresis. This is caused by manufacturing errors of the bump foil as well as by a small misalignment of bearing and shaft in the experimental setup.

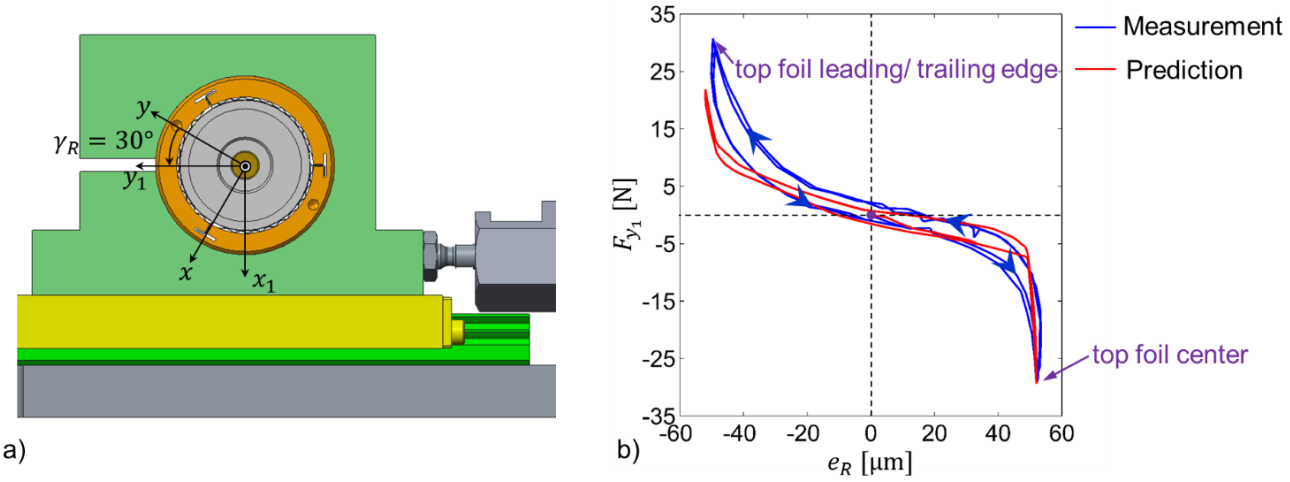

Fig. 6 Assembly orientation of the preloaded three-pad air foil journal bearing in measurement and simulation (a) as well as measurement and prediction of static hysteresis (b)

REFERENCES

[1] Heshmat, H., W. Shapiro, and S. Gray, *Development of foil journal bearings for high load capacity and high speed whirl stability.* Journal of Lubrication Technology, 1982. **104**(2): p. 149-156.

[2] Heshmat, H., J.A. Walowit, and O. Pinkus, *Analysis of Gas-Lubricated Foil Journal Bearings.* Journal of Lubrication Technology, 1983. **105**: p. 647-655.

[3] Kim, D., *Parametric Studies on Static and Dynamic Performance of Air Foil Bearings with Different Top Foil Geometries and Bump Stiffness Distributions.* Journal of Tribology, 2007. **129**(2): p. 354.

[4] Ku, C.-P.R. and H. Heshmat, *Compliant Foil Structural Stiffness Analysis: Part I - Theoretical Model Incluing Strip and Variable Bump Foil Geometry.* Journal of Tribology, 1992. **114**: p. 394-400.

[5] Ku, C.P.R. and H. Heshmat, *Structural Stiffness and Coulomb Damping in Compliant Foil Journal Bearings: Theoretical Considerations.* Tribology Transactions, 1994. **37**(3): p. 525-533.

[6] Le Lez, S., M. Arghir, and J. Frene, *A New Bump-Type Foil Bearing Structure Analytical Model.* Journal of Engineering for Gas Turbines and Power, 2007. **129**(4): p. 1047-1057.

[7] Aksoy, S. and M.F. Aksit, *A fully coupled 3D thermo-elastohydrodynamics model for a bump-type compliant foil journal bearing.* Tribology International, 2015. **82**: p. 110-122.

[8] Reissner, E., *On One-Dimensional Finite-Strain Beam Theory: the Plane Problem.* Journal of Applied Mathematics and Physics (ZAMP), 1972. **23**(5): p. 795-804.

[9] Libai, A. and J.G. Simmonds, *The nonlinear theory of elastic shells*. 2005: Cambridge university press.

[10] Bertsekas, D.P., *Constrained optimization and Lagrange multiplier methods*. Computer Science and Applied Mathematics. 1982, San Diego: Academic Press, Inc.

[11] Wriggers, P., *Computational Contact Mechanics*. 2006, Berlin, Heidelberg: Springer-Verlag.

KEYWORDS

Air Bearings, Foil Bearings, Journal Bearings